Electronic Supplementary Material (ESI) for Journal of Materials Chemistry C.

In situ monitoring drying process to disclose the correlation between molecular weights of polymer acceptor with flexible spacer and performance of all-polymer solar cells

Jiale Xiang,[a,b] Sven Englund,[a] Zewdneh Genene,[c] Guanzhao Wen,[d] Yanfeng Liu,*[a,e] Nannan Yao, [a,f] Rui Zhang,[a] Leiqiang Qin,[a] Lei Wang,[a] Ergang Wang,*[c] Wei Zhang,*[d] Fengling Zhang*[a, b]

1. Supporting Figures

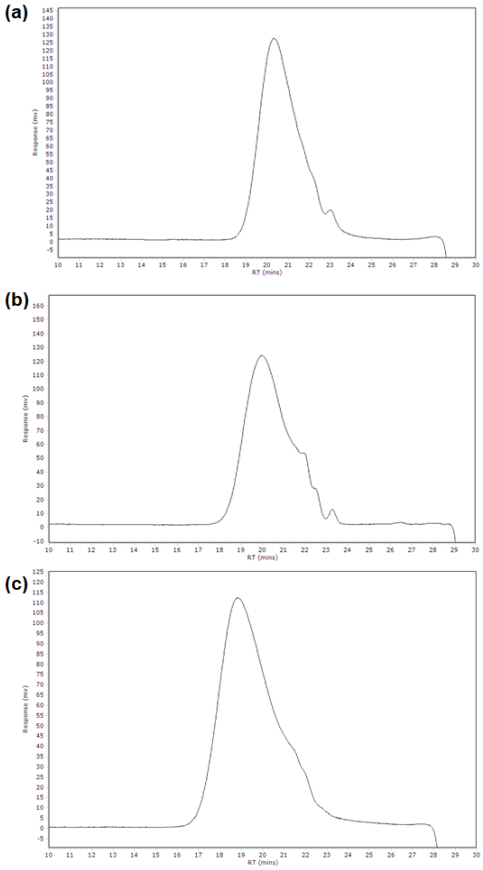

Figure S1. GPC profiles of PYTS samples with different molecular weight, (a) $PYTS_L$, (b) $PYTS_M$ and (c) $PYTS_H$.

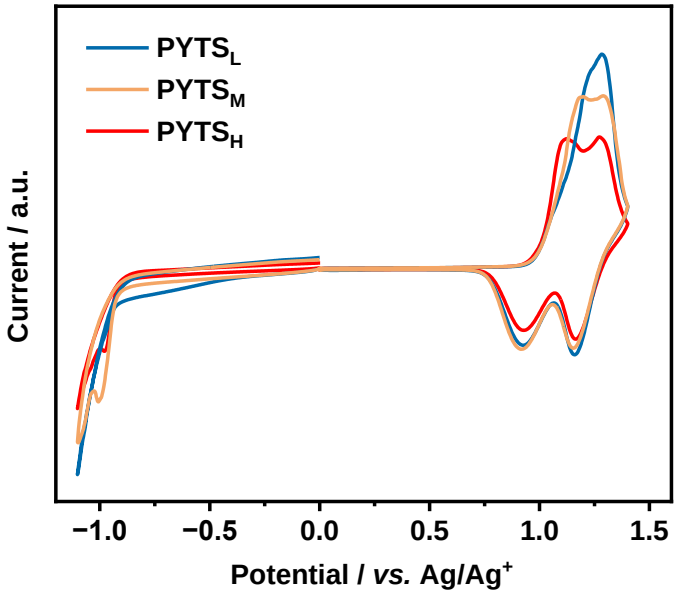

Figure S2. Cyclic voltammogram for reduction of PYTS thin film of different molecular weights.

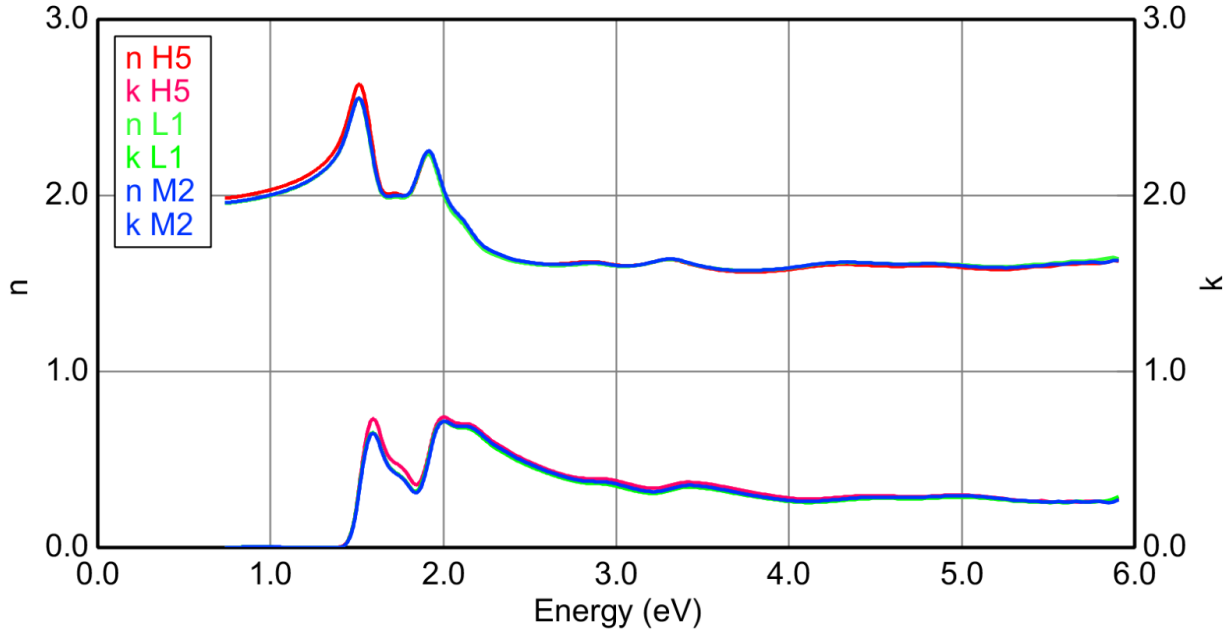

Figure S3. n, k values of PYTS with different M_n. L1 represents $PYTS_L$, M2 represents $PYTS_M$, H5 represents $PYTS_H$.

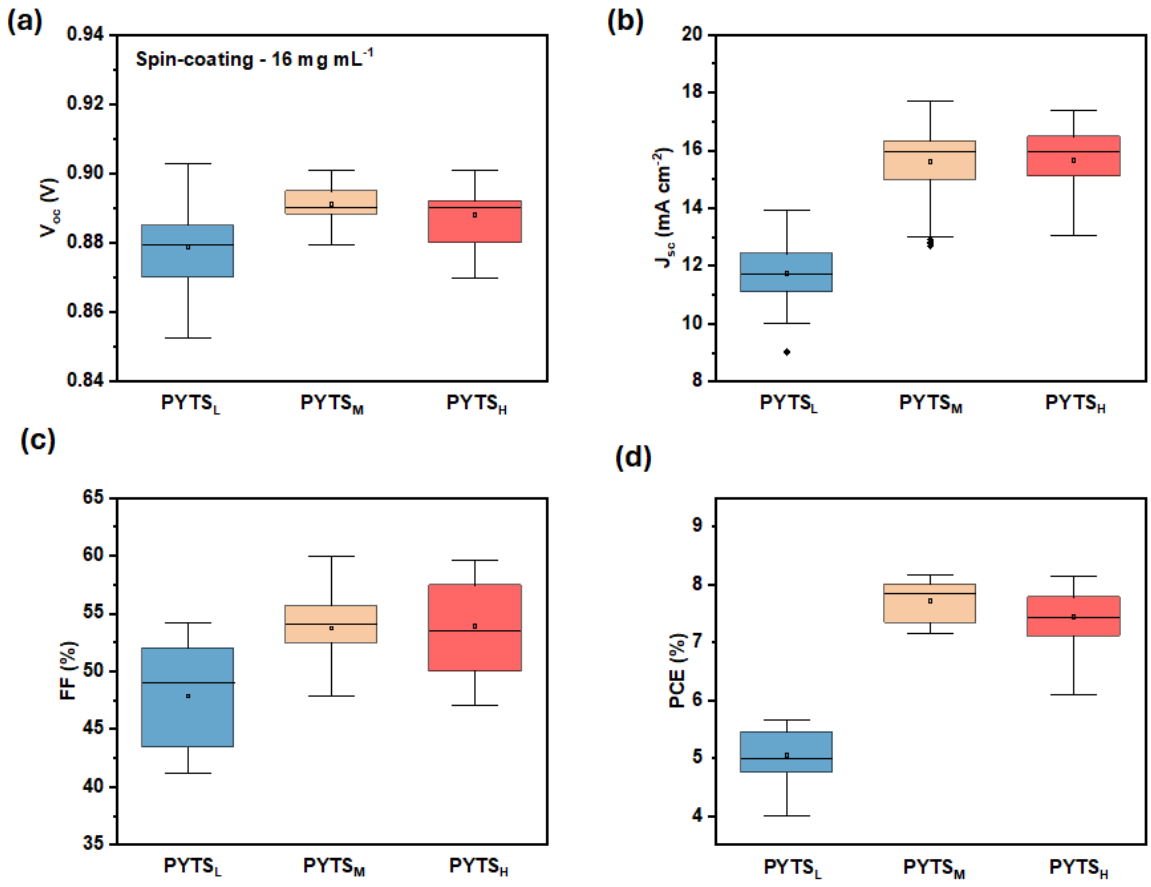

Figure S4. The relationships of photovoltaic parameters (V_{oc}, J_{sc}, *FF*, and *PCE*) with the M_n of acceptor polymer PYTS in PBDB-T:PYTS all-PSC devices with concentration of 16 mg mL^{-1} via spin-coating: (a) V_{oc}, (b) J_{sc}, (c) *FF*, and (d) *PCE*. The error bars were generated from over 24 devices at each M_n.

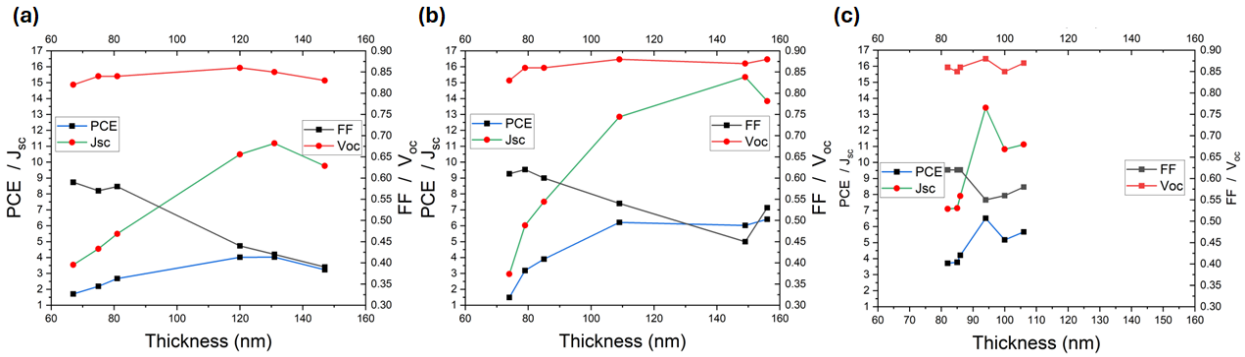

Figure S5. The relationships of photovoltaic parameters (V_{oc}, J_{sc}, *FF*, and *PCE*) with the thickness of active layer in PBDB-T:PYTS all-PSC devices via blade-coating: (a) $PYTS_L$, (b) $PYTS_M$, and (c) $PYTS_H$.

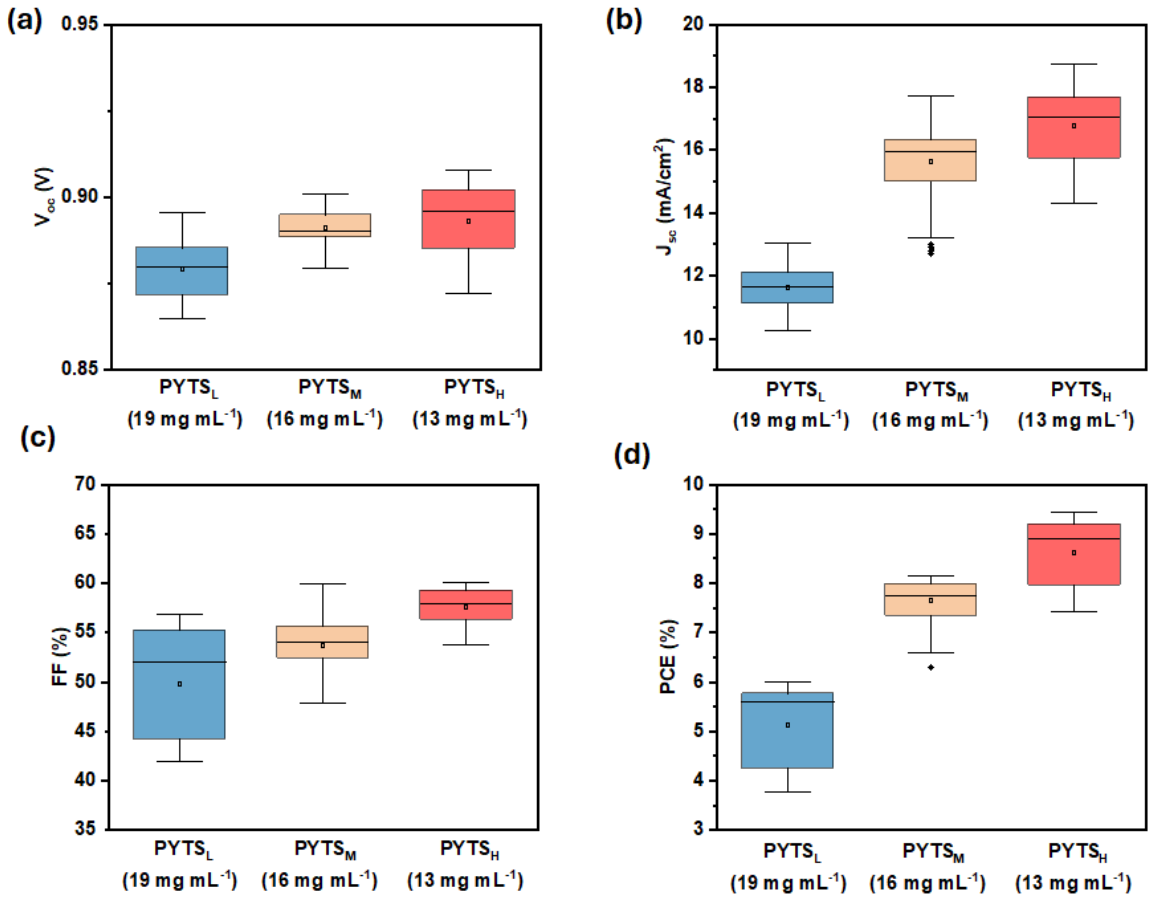

Figure S6. The relationships of photovoltaic parameters (V_{oc}, J_{sc}, *FF*, and *PCE*) with the M_n of acceptor polymer PYTS in PBDB-T:PYTS all-PSC devices with different concentration via spin-coating: (a) V_{oc}, (b) J_{sc}, (c) *FF*, and (d) *PCE*. The error bars were generated from over 24 devices at each M_n.

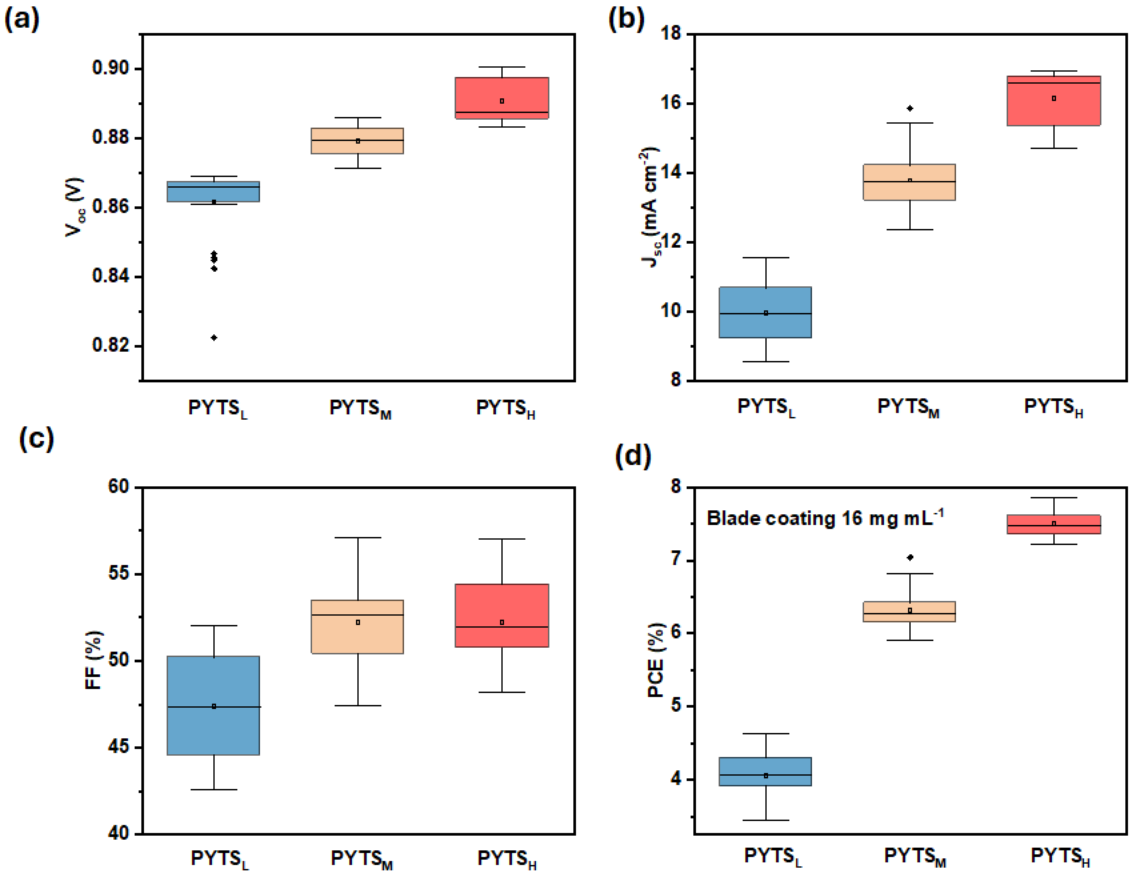

Figure S7. The relationships of photovoltaic parameters (V_{oc}, J_{sc}, *FF*, and *PCE*) with the M_n of acceptor polymer PYTS in PBDB-T:PYTS all-PSC devices with concentration of 16 mg mL^{-1} via blade-coating: (a) V_{oc}, (b) J_{sc}, (c) *FF*, and (d) *PCE*. The error bars were generated from over 24 devices at each M_n.

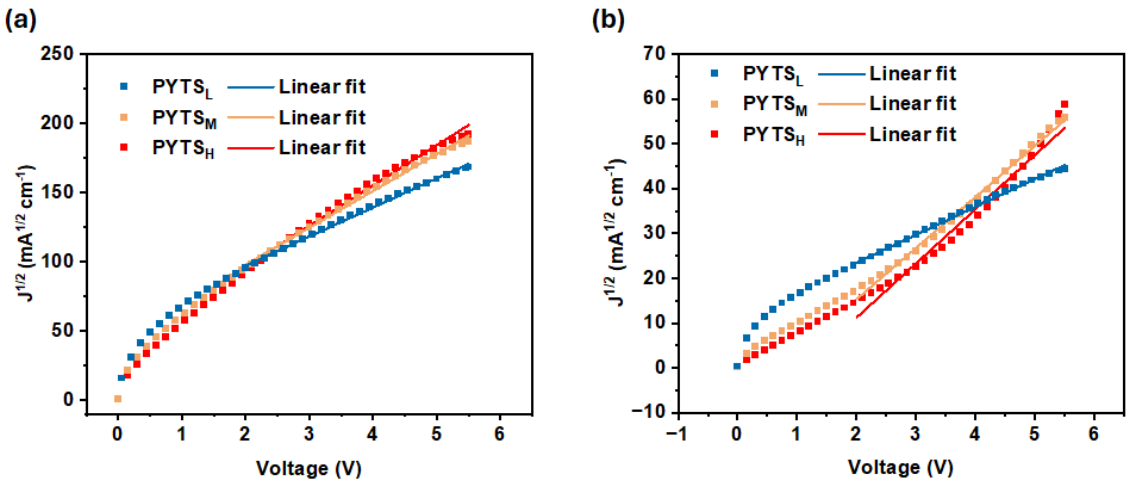

Figure S8. $J^{0.5}$ -V curves of the (a) hole-only and (b) electron-only devices derived from SCLC.

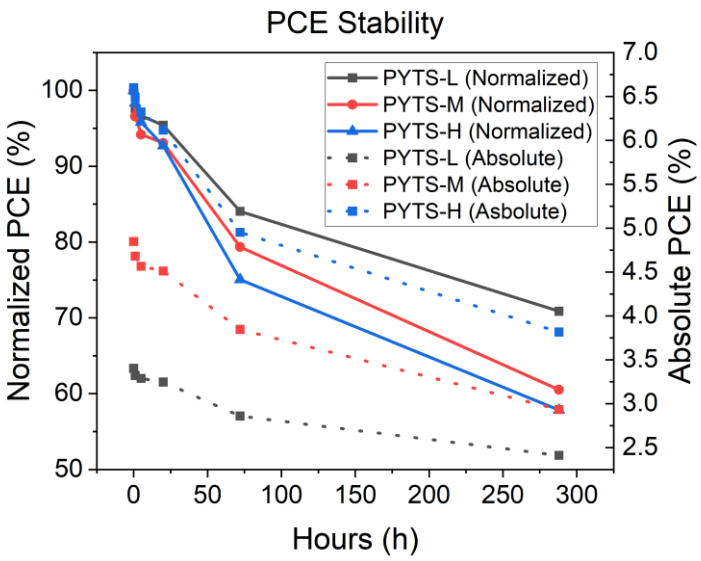

Figure S9. Storage stability of all-PSCs with different M_n, devices were stored in ambient air after encapsulation.

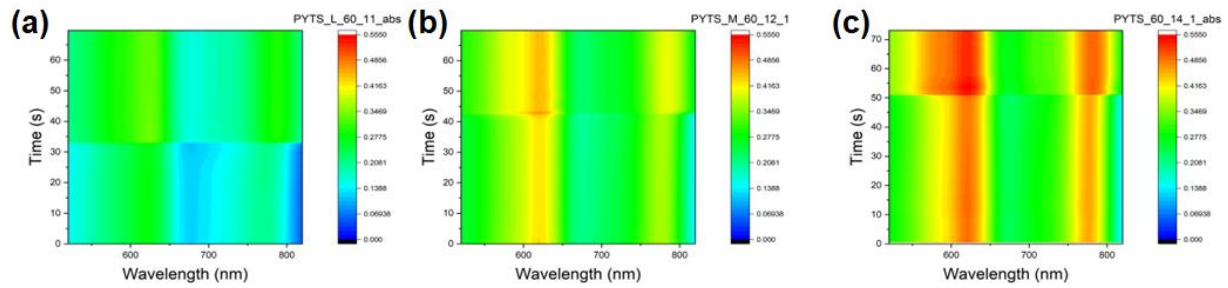

Figure S10. Time-dependent contour maps of UV-vis absorption spectra measured on different blends. (a) PBDB-T:$PYTS_L$, (b) PBDB-T:$PYTS_M$, and (c) PBDB-T:$PYTS_H$.

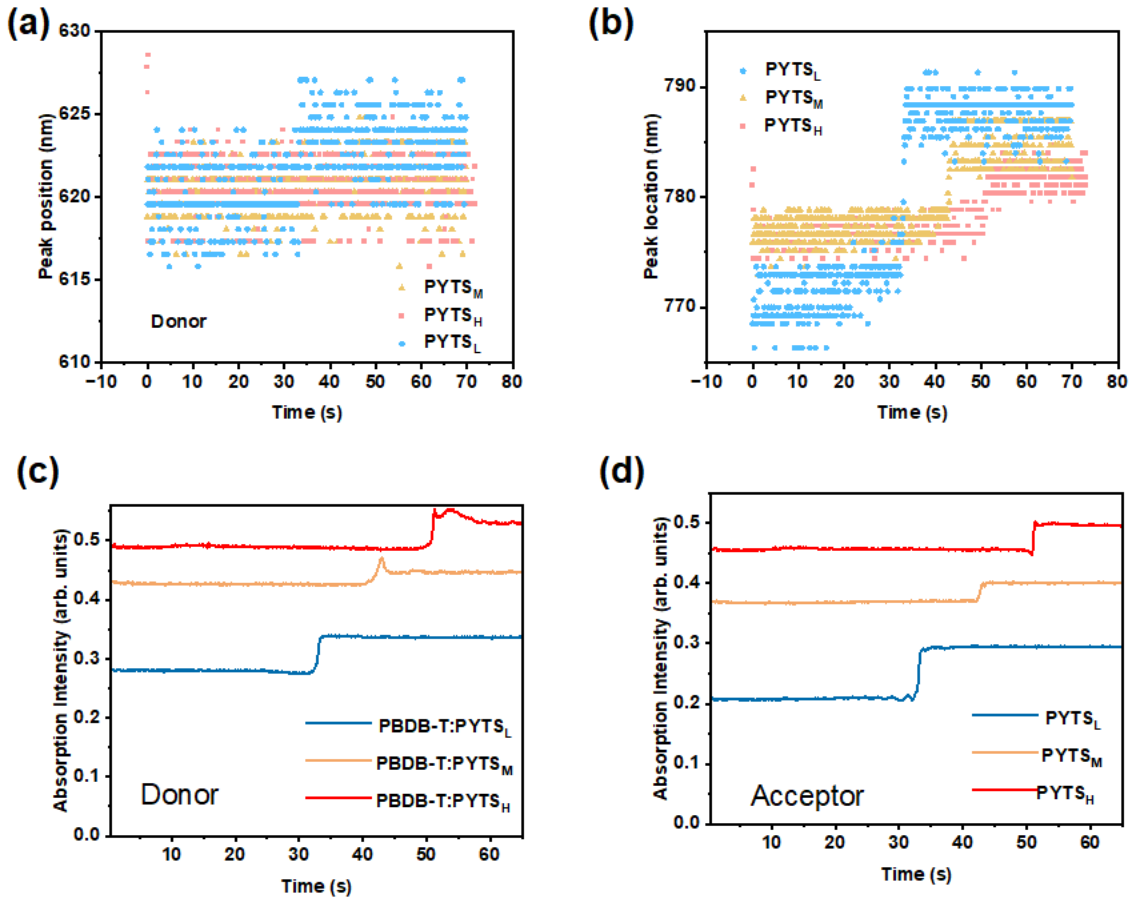

Figure S11. Plots of spectral evolution probed at the (a) donor and (b) acceptor absorption peaks based on the results in time-dependent contour maps.

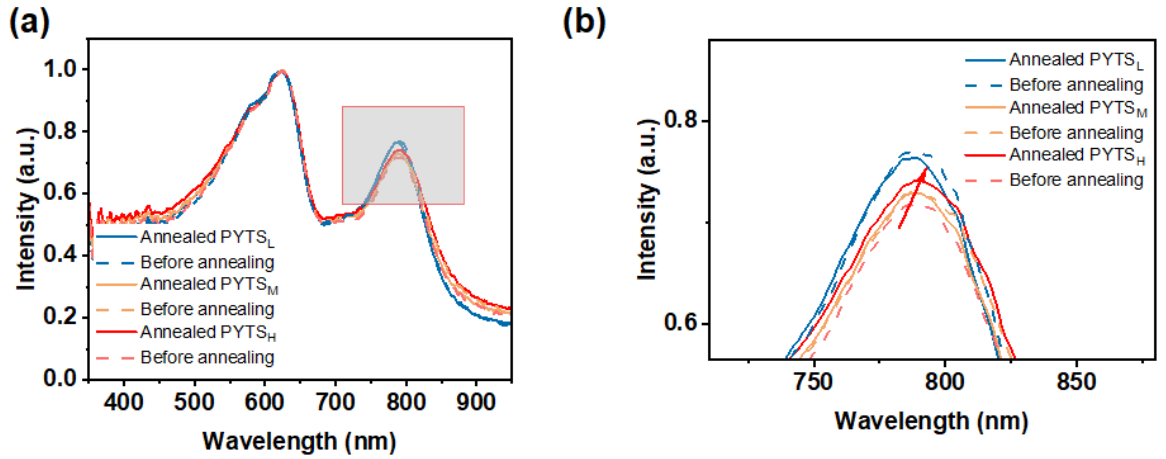

Figure S12. (a) Thin-film optical absorption spectra of the PBDB-T:PYTS acceptor copolymer at different number-average molecular weights Mn before and after heat annealing. (b) The enlarged view of the gray area in (a).

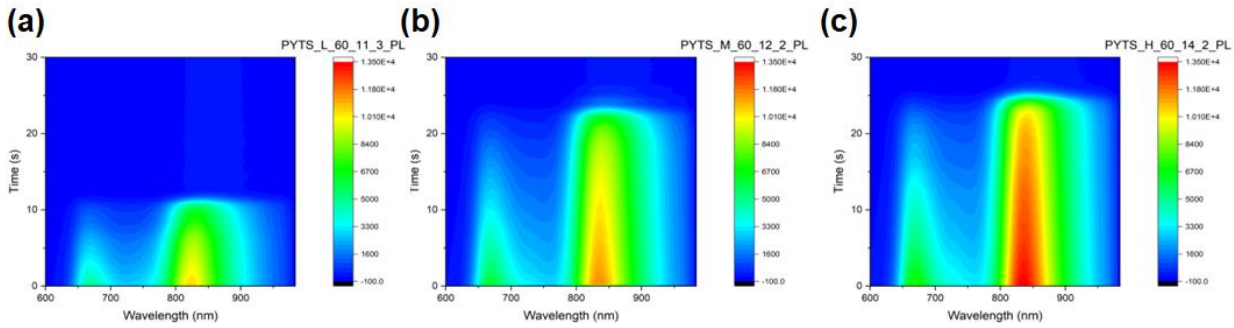

Figure S13. Time-dependent contour maps of PL spectra measured on different blends. (a) PBDB-T:PYTS$_L$, (b) PBDB-T:PYTS$_M$, and (c) PBDB-T:PYTS$_H$.

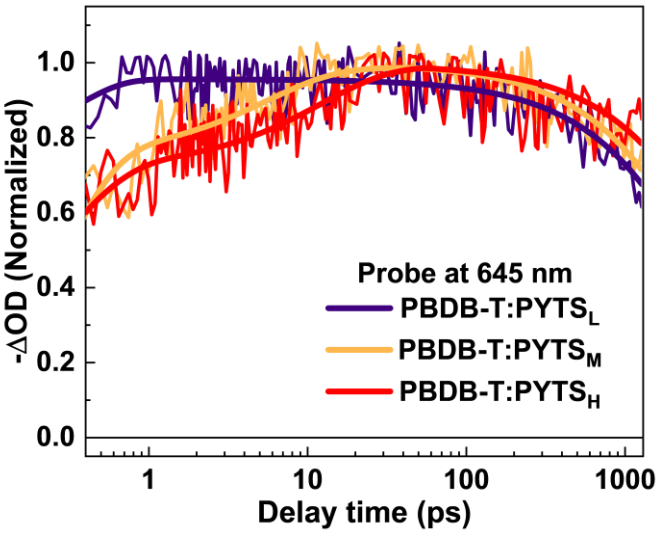

Figure S14. The extracted TA kinetics of ~645 nm of three blend films after excitation at 800 nm with an excitation fluence of 3.6 × 10^{13} photons·cm^{-2}·$pulse^{-1}$.

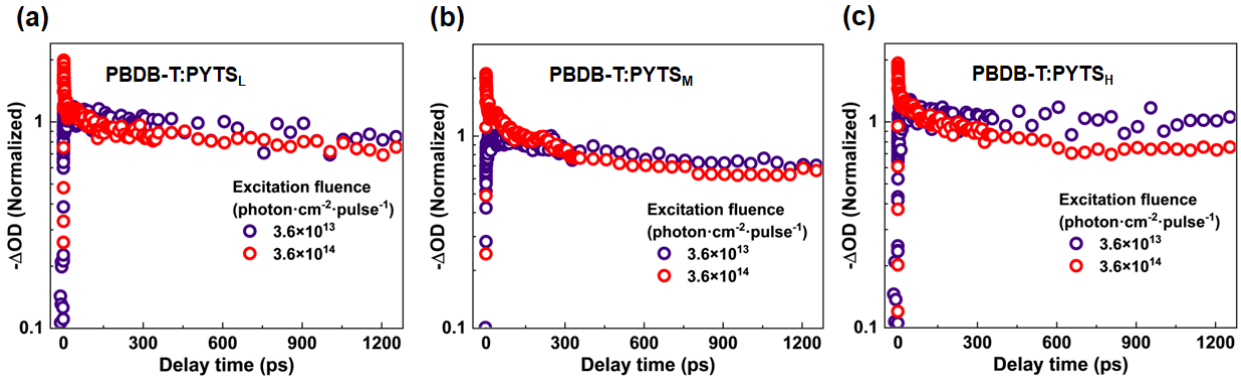

Figure S15. The extracted TA kinetics of ~645 nm of three blend films after excitation at 800 nm with various excitation fluencies. The TA kinetics normalized at ~30 ps.

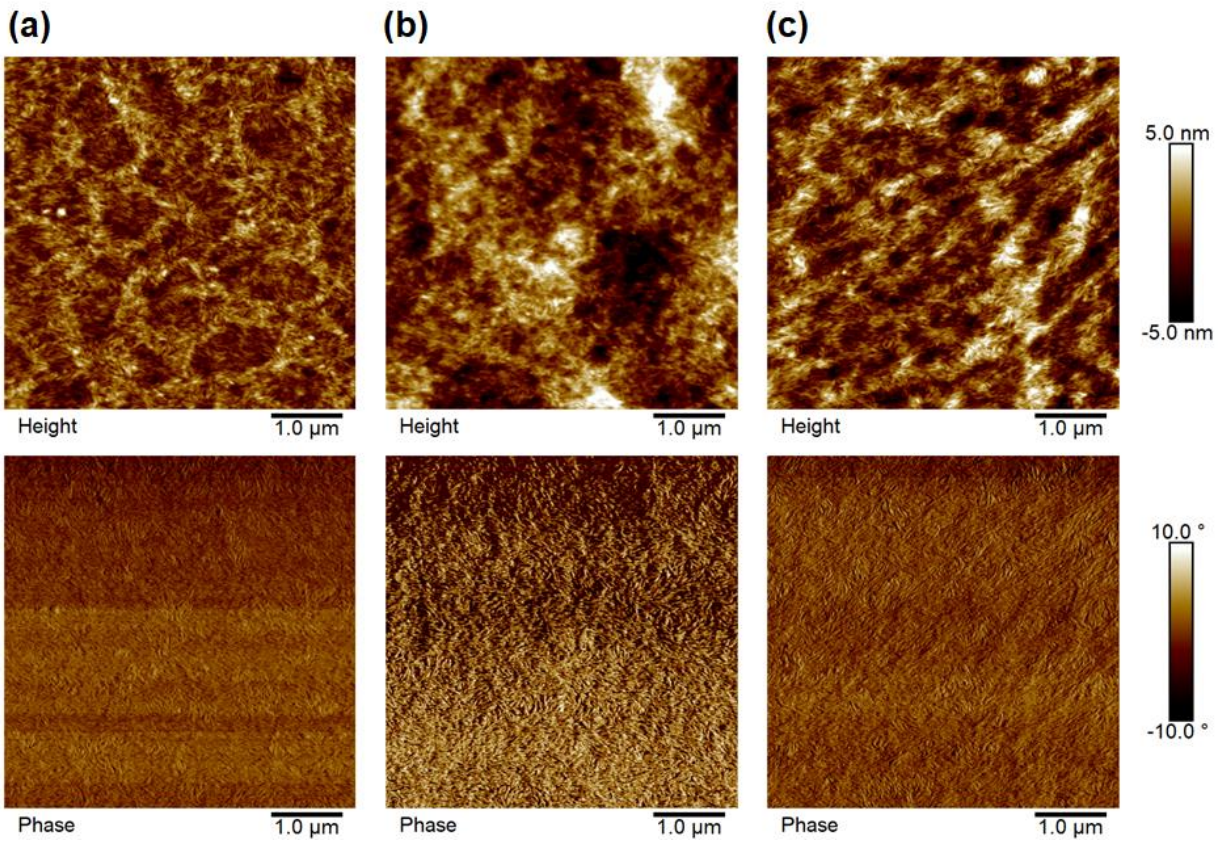

Figure S16. AFM height and phase images. (a) PBDB-T:PYTS$_L$, (b) PBDB-T:PYTS$_M$, and (c) PBDB-T:PYTS$_H$.

2. Supporting Tables

Table S1. PV performances of the all-PSCs depending on the Mn of P_As with concentration of 16 mg mL^{-1} via spin-coating.

	V_{oc} (V)	J_{sc} (mA cm^{-2})	*FF*(%)	*PCE* (%)
PBDB-T:$PYTS_L$	0.88 (0.88±0.01)	12.80 (11.74±0.93)	50.13 (47.86±4.33)	5.67 (5.05±0.39)
PBDB-T:$PYTS_M$	0.90 (0.89±0.01)	16.21 (15.61±1.17)	55.93 (53.73±2.45)	8.16 (7.71±0.33)
PBDB-T:$PYTS_H$	0.89 (0.89±0.01)	17.35 (15.68±1.05)	52.70 (53.89±3.62)	8.14 (7.44±0.46)

Table S2. PV performances of the all-PSCs depending on the Mn of P_As with concentration of 16 mg mL^{-1} via blade-coating.

	V_{oc} (V)	J_{sc} (mA cm^{-2})	*FF*(%)	*PCE* (%)
PBDB-T:$PYTS_L$	0.87 (0.86±0.01)	11.27 (9.96±0.86)	47.35 (47.40±3.06)	4.62 (4.05±0.29)
PBDB-T:$PYTS_M$	0.88 (0.88±0.00)	15.43 (13.78±0.81)	51.90 (52.23±2.38)	7.04 (6.32±0.24)
PBDB-T:$PYTS_H$	0.90 (0.89±0.01)	16.89 (16.16±0.72)	51.76 (52.19±2.43)	7.85 (7.50±0.18)

Table S3. The detailed fitting parameters of the rising process in ~645 nm for three blend films after excitation at 800 nm.

Active layer	A_1	τ_1 (ps)	A_2	τ_2 (ps)
PBDB-T:PYTS$_L$	/	/	/	/
PBDB-T:PYTS$_M$	0.76	0.21	0.23	5.70
PBDB-T:PYTS$_H$	0.71	0.27	0.27	12.32

Table S4. The detailed fitting parameters of charge recombination process for three blend films after excitation at 800 nm and probe at ~645 nm.

Active layer	A	τ (ps)
PBDB-T:PYTS$_L$	0.96	3756.89
PBDB-T:PYTS$_M$	0.99	3884.01
PBDB-T:PYTS$_H$	0.99	5450.44

Table S5. Detailed data of GIWAXS Characterization.

	(100)				(010)			
	Position (Å^{-1})	FWHM(Å^{-1})	Distance (Å)	CCL (Å)	Position (Å^{-1})	FWHM (Å^{-1})	Distance (Å)	CCL (Å)
PBDB-T:PYTS$_L$	0.281	0.089	22.44	78.44	1.66	0,434	3.78	16.08
PBDB-T:PYTS$_M$	0.281	0.085	22.44	82.13	1.68	0,395	3.74	17.67
PBDB-T:PYTS$_H$	0.281	0.095	22.44	73.48	1.68	0,319	3.74	21.88